JGR Oceans

RESEARCH ARTICLE
10.1029/2022JC019218

Key Points:

- A modified arrested topographic wave model is used to quantify relative contributions of local wind and open-ocean forcing
- The penetration of open-ocean signals to the coast can be estimated based on the proposed "basin-to-coast" dynamical linkage framework
- Reconstructed sea levels agree well with tide-gauge measurements at the west coasts of North Pacific and North Atlantic

Correspondence to:
H. Lin, and J. Hu,
hylin@xmu.edu.cn;
hujy@xmu.edu.cn

Citation:
Lin, W., Lin, H., Hu, J., & Huang, L. (2022). Relative contributions of open-ocean forcing and local wind to sea level variability along the west coasts of ocean basins. *Journal of Geophysical Research: Oceans*, *127*, e2022JC019218. https://doi.org/10.1029/2022JC019218

Received 21 AUG 2022
Accepted 15 NOV 2022

Relative Contributions of Open-Ocean Forcing and Local Wind to Sea Level Variability Along the West Coasts of Ocean Basins

Wenqiang Lin[1], Hongyang Lin[2], Jianyu Hu[2], and Lingfeng Huang[1]

[1]State Key Laboratory of Marine Environmental Science, College of the Environment and Ecology, Xiamen University, Xiamen, China, [2]State Key Laboratory of Marine Environmental Science, College of Ocean and Earth Sciences, Xiamen University, Xiamen, China

Abstract This study aims to reconstruct sea level at the coast by quantifying relative contributions of local wind forcing and the penetrated open-ocean signals, and thus to build a dynamical connection that seamlessly links the ocean basin to the coast. A linear, modified arrested topographic wave (ATW) model is used to examine the transmission of interior sea level across the continental shelf and the role of alongshore wind in determining the coastal sea level. The local wind stress substantially influences the coastal sea level but does not affect the transmission of open-ocean signals in the linear framework. Increased bottom friction or gentler slope of shelf favors the penetration of open-ocean signals. This modified ATW model is then applied to the shelf seas of North Pacific and North Atlantic, with model parameters being set according to the realistic features of regional oceanography. The offshore boundary condition is determined by the integrated barotropic and baroclinic ocean responses in the ocean basin and the transmission processes across western boundary currents. Based on the proposed "basin-to-coast" dynamical linkage framework, one can estimate the relative contributions of open-ocean forcing and local wind to the total coastal sea level. According to these partitions, the reconstructed coastal sea levels along the west coasts of North Pacific and North Atlantic on seasonal time scale are in close agreement with tide-gauge observations. The idea and specific calculations of coastal sea level reconstruction could be readily applied to other coasts of the global ocean.

Plain Language Summary This study aims to reconstruct sea level at the coast by quantifying relative contributions of local wind forcing and the penetrated open-ocean signals. The contribution of local wind to coastal sea level is estimated by a linear model, while the contribution of the remote open-ocean forcing is grounded on a "basin-to-coast" dynamical linkage framework. Applying the above model to the East China Sea, we find that the penetration ratio of open-ocean signals is 0.63, which contributes 34% of the total coastal sea level; the remaining contribution (66%) is induced by the local alongshore wind. The coastal sea level is then reconstructed based on these partitions, and shows a good agreement with the observed monthly sea level from tide gauges. We also apply the framework to reconstruct sea level at the west coast of North Atlantic, and the reconstruction also agrees well with observations. The success in the two applications proves reliability of the proposed dynamical linkage framework, and also provides a promising guide to monitor/forecast sea level at the coast given simply the local and remote wind fields.

1. Introduction

The penetration or transmission of open-ocean signals onto the coast is an important issue both scientifically and practically. From the scientific point of view, it is a dynamically subtle problem to investigate roles of the continental slope/shelf and the western boundary currents in affecting the transmission of open-ocean forcing. From the practical point of view, it would be of great significance to monitor signal changes in the ocean basin interior via tide-gauge stations at the coast. Reliable prediction of signals at the coast requires better understanding of local forcing as well as the on-shelf penetration processes of the open-ocean forcing.

A number of studies have examined the manifestation of open-ocean forcing on the adjacent slope/shelf or coast. Huthnance (1992) provided a comprehensive review of the on-shelf penetration of oceanic flow structures and hence shed important lights on coastal monitoring of oceanic circulation taking the remote forcing into account. By using the arrested topographic wave (ATW) theory, Csanady (1982) and Hughes et al. (2019) concluded that coastal tide gauges can only monitor oceanic motions with scales of thousands of kilometers. Huthnance (2004)

used a more realistic model and suggested that coastal sea level responds more effectively to the largest-scale oceanic motion (typically thousands of kilometers). These studies indicate that short-wavelength variability of open-ocean signals does not penetrate across the shelf. In fact, the western boundary of ocean basin was found to be the graveyard for mesoscale eddies propagating from the east (Zhai et al., 2010); they interpreted that eddy energy can be transferred to high-wavenumber vertical modes when eddies impinge on the sloping topography near the western boundary. Mesoscale variability in the deep ocean is also shown to be strongly damped at the continental slope, as evidenced by the coherence of bottom pressure variations over along-shelf distances of tens of thousands of kilometers (Hughes et al., 2018). The coast acts as a low-pass filter in wavenumber for sea level signals from the nearby deep ocean.

With the betterment of geodetic approach, a sequence of recent studies have demonstrated that the coastal sea level variability can markedly differ from the variability in the nearby deep ocean because of the presence of continental shelf/slope (Higginson et al., 2015; Lin et al., 2015; Woodworth et al., 2019). Wright (1986) and Middleton (1987) pointed out that a gentle continental slope would effectively insulate the continental shelf from the influence of a deep ocean pressure gradient. Huthnance (1987) suggested that oceanic sea level features of short scale do not penetrate fully onto the coast due to the presence of a continental slope/shelf, and Huthnance (2004) found the similar results with a linear model which includes continuous vertical stratification and focuses on the shelf and slope. In particular, Higginson et al. (2015) showed that the steep sea level tilt in deep ocean, with a drop of ∼1 m across Gulf Stream, is missing at the coast, where a mild drop of about 0.2 m is detected at Cape Hatteras where the shelf is broad. Recently, Wise et al. (2018, 2020) showed that narrower continental shelves and larger bottom friction would increase the penetration of deep ocean variability onto the coast.

Although inclusions of the continental shelf/slope and bottom friction can significantly alter the transmission of interior sea level to the coast and then reshape the tilt of coastal sea level, the ocean response over the continental shelf to an additionally imposed along-shelf wind stress still remains unclear. On the one hand, Csanady (1978) found the alongshore pressure gradient imposed at the offshore boundary by the adjacent open-ocean forcing produces exactly the type of response observed over the eastern North American continental shelf, implying that the local wind stress plays a limited role in the coastal sea level tilt. Hence, the model used by Wise et al. (2018) and Hughes et al. (2019) ignored the wind stress as the boundary condition at the coast. On the other hand, Lin et al. (2021) proposed that wintertime coastal sea level tilt along the coast of the Chinese mainland is mainly affected by the strong alongshore wind stress rather than the open-ocean forcing. Yang and Chen (2021) also suggested that the local wind stress has more direct impacts on the along-shelf sea level gradient in the shallower water of the Northwest Atlantic Ocean. Therefore, further investigations are required to unravel the influence of the local wind stress on the coastal sea level.

Limited attempts have been made to reconstruct coastal sea level from both local and remote contributors. Based on a linear least-squares regression, Li and Xu (2020) obtained a polynomial equation to reconstruct the coastal sea level using signals from the ocean interior, atmospheric forcing, and the local steric effect. They considered the transmission of open-ocean signals across the western boundary current following the theory of Minobe et al. (2017), but did not include the on-shelf penetration processes since they applied the reconstruction along the Pacific coast of Japan where the shelf is narrow and steep. In addition, it would be difficult to diagnose specific dynamics based simply on statistical reconstruction from linear regression. In this study, we are more interested in whether the open-ocean signals, combined with the varying alongshore wind stress, could be used to dynamically predict the sea level at the coast. To this end, we need to partition the coastal sea level into components contributed by the local wind and the penetrated portion of open-ocean signals. Our approach is to recall a linear, *f*-plane model (Csanady, 1978) with realistic alongshore wind stress and open-ocean boundary conditions. One of the novelties is that we simultaneously take the local alongshore wind stress and the remote open-ocean forcing into account; the former is often ignored in previous similar studies (e.g., Hughes et al., 2019; Wise et al., 2018) but could be quite important in the coastal sea level reconstruction.

Such a coastal reconstruction requires understanding of (a) sea level propagation in the open ocean via for example, Rossby waves, (b) transmission across the western boundary current and continental slope, and (c) eventually the shore-ward penetration on the continental shelf (Figure 1). Our goal is to build a dynamical connection to seamlessly link the vast interior ocean basin all the way to the coast. We will first take the western coast of the East China Sea (ECS; a marginal sea of the North Pacific) as a testbed to perform the coastal sea level reconstruction by considering the response to the local wind, and the effect of bathymetry/friction on the transmission of

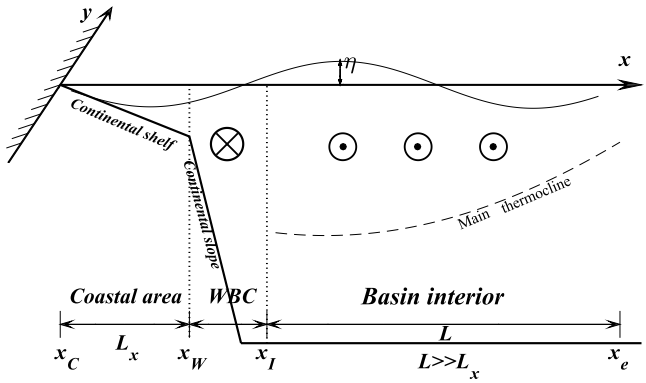

Figure 1. Schematic illustrating the coordinates and the interaction among the idealized domains, including the basin interior (i.e., ocean interior), western boundary current (WBC, i.e., western boundary layer), and the coastal area of our interest in this study. The positive y points poleward. The circles with dots indicate interior Sverdrup transport, and the circle with a cross denotes the poleward western boundary current. η is the sea surface height. L_x and L are the cross-shore width of continental shelf and ocean basin ($L >> L_x$). x_C, x_W, x_I, and x_e are the zonal positions of the coast, the west wall of western boundary current, the western end of ocean interior, and the eastern boundary of ocean interior, respectively.

interior sea level. To validate the reconstruction paradigm, we apply the same calculation procedure to reconstruct sea level at the western coast of North Atlantic. As noted by Stommel and Leetmaa (1972), the physical processes of sea level transmission on the continental shelf are location dependent, but our reconstruction logic (detailed below) could be readily applied to other regions around the world coasts.

This paper is organized as follows. Section 2 describes the data used to estimate the response of sea level. In Section 3, the modified ATW model and sensitivity experiments will be presented to examine the effects of the shelf steepness, bottom friction, and alongshore wind stress. In Section 4, we quantitatively assess the contributions of the open-ocean forcing and the alongshore wind stress forcing, and then reconstruct sea level at the coast. Section 5 includes the discussion and summary.

2. Data

2.1. Sea Level Observational Records

Monthly sea level data records at tide gauges along the west coasts of North Pacific and North Atlantic are obtained from the Permanent Service for Mean Sea Level (PSMSL; Holgate et al., 2013), which constructs the "revised local reference" (or "RLR") data set that has been reduced to a common datum for each station. Locations of the tide-gauge stations are shown in Figure 2. We remove the time-mean value for sea level time series at each individual station. The tide-gauge measurements at the west coasts of ECS (Figure 2a: Kanmen) and North Atlantic (Figure 2b: Charleston and Fernandina Beach) will be used to compare with the reconstructed sea levels. Sea level records at station Nisinoomote will be used to calculate the sea level at the west wall of the western boundary current (x_W in Figure 1) (see details in Section 4). This station is located on an island, close enough to the Kuroshio; the nearby narrow and steep continental shelf can be considered approximately as a vertical sidewall, in accord with the assumption of an ocean bounded by vertical sidewalls in the theory of Minobe et al. (2017).

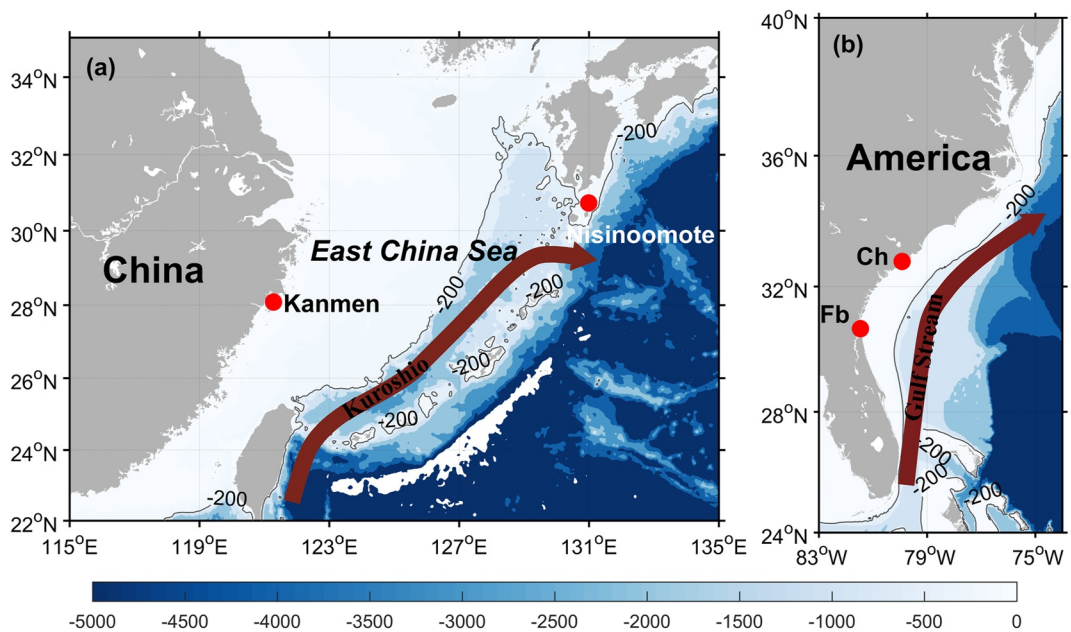

Figure 2. Study areas and locations of tide-gauge stations. Color shading shows the bathymetry (in m) and gray lines indicate the 200-m isobaths. Ch and Fb denote the Charleston tide-gauge station and Fernandina Beach tide-gauge station, respectively. Bold carmine arrows indicate the pathway of the western boundary currents (Kuroshio and Gulf Stream).

2.2. Atmospheric Pressure Data and the IB Effect

The response of sea level to fluctuating atmospheric pressure loads is a static (inverted barometer; IB) effect (η_{IB}) (Wunsch & Stammer, 1997). We estimate the IB effect by $\eta_{IB} = -(P - P_{ref})/\rho_0 g$, where $\rho_0 = 1{,}027$ kg m^{-3} is water density, $g = 9.8$ m s^{-2} is the gravity acceleration, $P_{ref} = 1010.9$ hPa is the spatial average of pressure over the global ocean, and P is the local atmospheric pressure. 1 mbar increase in sea surface pressure corresponds to ∼1 cm depression in local sea level. The monthly sea level pressure is obtained from the NCEP/NCAR (National Centers for Environmental Prediction and National Center for Atmospheric Research) reanalysis data (Kalnay et al., 1996). The monthly sea level pressure data set over 1992–2010 is used to calculate η_{IB} closest to the tide-gauge stations.

2.3. Wind Stress

We use the monthly wind stress data from NCEP Climate Forecast System Reanalysis (NCEP/CFSR), which provides the estimate of a global, high-resolution coupled atmosphere-ocean-land surface-sea ice system over 1979–2010 with a horizontal resolution of about 0.3° (Saha et al., 2010).

3. Modeling Approach

3.1. Formulation

We consider a long and straight coastline, with y axis coinciding with the coast, positive y pointing poleward and positive x pointing offshore (Figure 1). The depth of the shelf h is assumed to be only a function of offshore distance, i.e., $h = h(x)$. That is, h is uniform alongshore. The slope of the shelf is assumed to be constant for simplicity, i.e., $dh/dx = s$. The density field is also assumed to be homogeneous and the bottom friction is taken to be linearly proportional to the depth-averaged velocity. The offshore components of the surface and bottom stresses are negligible compared to the Coriolis force of alongshore flow. Hence, we consider the cross-shore momentum equation to be in geostrophic balance while retaining the frictional stresses in the alongshore momentum equation, a model considered in Csanady (1978). The steady-state, linear, depth-averaged momentum equation, and mass continuity equation can be written as

$$-fv = -g\frac{\partial \eta}{\partial x} \tag{1a}$$

$$fu = -g\frac{\partial \eta}{\partial y} + \frac{F}{h} - \frac{rv}{h} \tag{1b}$$

$$\frac{\partial (uh)}{\partial x} + \frac{\partial (vh)}{\partial y} = 0 \tag{1c}$$

where f is Coriolis parameter and is constant, $g = 9.8$ m s^{-2} is gravitational acceleration, $\eta(x, y)$ is the surface elevation, $u(x, y)$ and $v(x, y)$ are cross-shore and alongshore components of velocity, respectively. The kinetic bottom stress is rv, where r is a bottom friction coefficient. $F = F(y)$, a function of alongshore distance only, is the alongshore component of the kinematic wind stress on the continental shelf. Equation 1b can be rewritten as $uh = -gh/f\ \partial\eta/\partial y + F/f - rv/f$, with terms on the right-hand side representing the geostrophic cross-shore transport, wind-driven Ekman transport, and bottom Ekman transport in the depth-integrated alongshore momentum balance, respectively.

Eliminating u and v from Equation 1, we obtain a single equation for the surface elevation η

$$\frac{\partial^2 \eta}{\partial x^2} + \frac{fs}{r}\frac{\partial \eta}{\partial y} = 0 \tag{2}$$

There are two lateral boundary conditions. The first is the no-normal-transport boundary condition at the coast, i.e., $uh = 0$, yielding

$$\frac{\partial \eta}{\partial x} = \frac{fF}{rg} \text{ at } x = 0 \tag{3}$$

What is different from the model of Csanady (1978) is that we consider an alongshore pressure gradient at the offshore edge of the shelf (x_W in Figure 1) as the second boundary condition on the offshore side (Huang, 2010; as we will also show below, it is an appropriate and simplified condition), which takes a sinusoidal form

$$\eta(L_x, y) = \eta_1 \sin(2\pi k y) \text{ at } x = L_x \tag{4}$$

where k is the wavenumber of the open-ocean signals, L_x is the cross-shore width of continental shelf, and η_1 is the amplitude of the open-ocean signals. We will refer to this model as the modified ATW model.

The model is configured on a horizontal 2-D rectangle region. The model parameters are first set to ideally represent the ECS, with the typical values of cross-shore width of $L_x = 200$ km, and alongshore length of $L_y = 1{,}500$ km. The horizontal grid is $\Delta x = \Delta y = 2$ km. The model (Equation 2) is numerically solved following the computational scheme of Skeel and Berzins (1990) that adopts a simple piecewise nonlinear Galerkin/Petrov-Galerkin method with a second-order accuracy in space. In this study, we run each experiment with long enough alongshore length (i.e., 15,000 km) to avoid initial influence from the northern boundary.

3.2. Characterization of the Modified ATW Model

We will use the modified ATW model to investigate the role of local wind and the transmission of open-ocean signals in setting up the coastal sea level. A set of sensitivity experiments will be configured to examine the factors that influence the transmission process and factors that influence the coastal sea level. Such factors include the spatial scale of the open-ocean signals and local wind, shelf width, shelf steepness, and bottom friction.

3.2.1. Transmission of Open-Ocean Signals

The alongshore wind stress is first set to be zero (i.e., $\partial\eta/\partial x = 0$ at $x = 0$), in order to isolate factors affecting the transmission of open-ocean signals. We now examine the model dependence on the spatial scale of open-ocean signals. The model parameters are set following previous studies: the cross-shelf slope s is 0.001 (implying the depth changes from 0 to 200 m over a shelf width of 200 km), the friction coefficient r is 1.5×10^{-3} m s^{-1}, and then Equations 2–4 are numerically solved with the wavelength of open-ocean signals being 750 and 1,500 km, respectively. Compared to the nearby open-ocean signals, coastal sea level signals are spatially smoothed, reduced in amplitude, and displaced equatorward along the coast (Figures 3a and 3b), as analogous to the steady advection-diffusion problem of a thermal fluid (Csanady, 1978). This feature has also been marked and explained by Wise et al. (2018) and Hughes et al. (2019). Comparison between Figures 3a and 3b indicates that larger-scale open-ocean signals result in greater penetration to the coast. This is further evidenced by Figure 3c, showing that the penetration ratio decreases gradually with increasing wavenumber of the offshore signals, although the decreasing rate also depends on the width of the shelf. Generally speaking, wider shelf tends to insulate the offshore signals more effectively. In other words, short wavelength variability of open-ocean forcing is more vulnerable to be insulated by the continental shelf/slope during on-shelf penetration, leaving the coast can only "feel" larger-scale signals from the open ocean.

We now examine the effect of shelf steepness and bottom friction on the penetration of interior sea level to the coast. Two groups of model sensitivity experiments are run with three values of the slope of shelf (s) and friction coefficient (r) for each group (Figure 4). Here, the interior sea level is assumed to be sinusoidal with an alongshore wavelength of 1,500 km (black lines in Figure 4). Model solutions indicate that the coastal sea level (color lines) for each case is reduced in amplitude with an equatorward displacement compared to the open-ocean signals. The model sensitivities further demonstrate that decreasing the slope of shelf, or increasing the bottom friction, would increase the penetration of interior sea level to the coast with less equatorward displacement. These results are in line with Wise et al. (2018) who found that the equatorward displacement of open-ocean signals is reduced with reduced depth of the active layer and increased bottom drag, and also in line with Huthnance (2004) who, by using a more sophisticated model, proved that friction aids oceanic signal transmission onto and across the continental shelf to the coast.

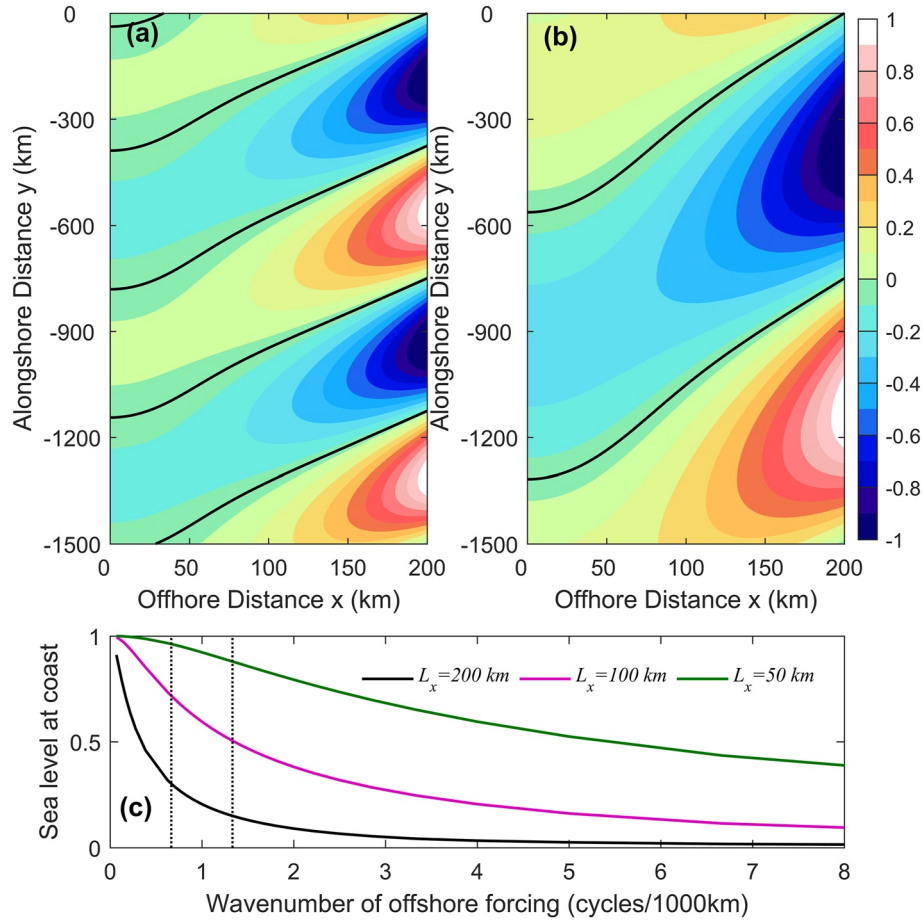

Figure 3. Coastal sea level responses to open-ocean forcing. The open-ocean boundary is at $x = 200$ km where sea level is taken to be $\eta\ (L_x,y) = -\sin(2\pi ky)$, and k is the alongshore wavenumber of (a) $k = 1/(750$ km) and (b) $k = 1/(1{,}500$ km). The black lines indicate zero contours. (c) The amplitude of sea level at coast as a function of the wavenumber of open-ocean forcing for different shelf widths L_x. The two dotted lines correspond to wavenumbers used in (a) and (b). The linear friction coefficient used in these cases is $r = 1.5 \times 10^{-3}$ m s^{-1}, the slope is $s = 0.001$ and the Coriolis parameter is $f = 10^{-4}$ s^{-1}. The northern boundary is at $y = 0$ and the equatorward boundary is at $y = -1{,}500$ km.

3.2.2. Role of Local Wind Stress

According to previous studies (e.g., Jan et al., 2002; Lin et al., 2021; Oey et al., 2014; Yang & Chen, 2021), the local wind forcing has nonnegligible impacts on the sea level along the coast. To elucidate the role of local alongshore wind stress on modulating the coastal sea level, we design three experiments. (a) The local wind stress is omitted and the model is forced only by the open-boundary condition with the wavelength of the open-ocean signal being 3,000 km; the coastal sea level is labeled η_O for this case (Figure 5a, red line). (b) The open-ocean signals are omitted and the model is forced only by local wind stress with the wavelength of the alongshore wind being 1,500 km (η_W; Figure 5a, blue line). (c) The model is forced by the local wind and open-ocean signals with the respective wavelength mentioned above (η_{O+W}; Figure 5a, black line). It is found that the sum of η_O and η_W (Figure 5a, green line) exactly coincides with η_{O+W}, which is expected since the model is linear. The results also indicate that in addition to the open-ocean signals, the local wind stress can significantly affect the coastal sea level and its alongshore tilt, yet would not affect the transmission of open-ocean signals in the linear regime. These findings also apply to the cases with different wavelengths of local wind stress and open-ocean forcing (not shown). Accordingly, the alongshore coastal sea level gradient is jointly modulated by the open-ocean forcing and the alongshore wind stress, providing partial evidence for the interpretation of Lin et al. (2021).

When the model is forced only by wind stress, the spatial distribution of sea level spreads offshore with an equatorward displacement (Figure 5b). Such wind-forced-only experiments are also run with varying wavelengths

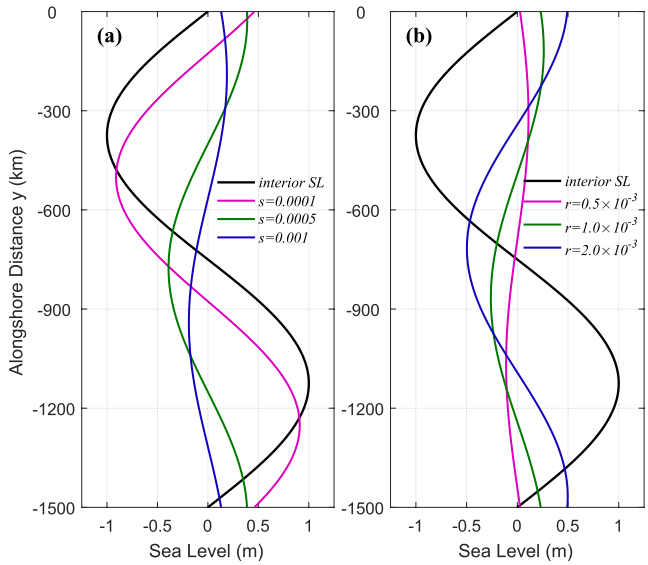

Figure 4. Sea level at the coast (color lines) derived from sensitivity experiments with varying slopes of the shelf (a) and friction coefficients (b). Black lines in both panels indicate interior sea level, which is taken to be $\eta(L_x, y) = -\sin(2\pi ky)$, and the alongshore wavelength is $1/k = 1{,}500$ km $y = 0$ and $y = -1{,}500$ km are the northern and southern boundaries of the model, respectively. The Coriolis parameter is $f = 10^{-4}$ s^{-1} and the alongshore wind stress is set to zero.

of alongshore wind stress (Figure 5c), friction coefficients (Figure 5d), and slopes of the shelf (Figure 5e). Overall, larger-scale alongshore wind stress, smaller bottom friction, and/or gentler slope is associated with larger amplitude of coastal sea level and its alongshore tilt. A complete list of model parameters for all the sensitivity experiments shown in all panels of Figure 5 is summarized in Table 1.

Through a set of sensitivity experiments shown above, our simple model highlights the importance of both the alongshore wind stress (local forcing) and open-ocean signals (remote forcing) in driving the coastal sea level. It is interesting to compare the dependence of local and remote forcings (i.e., alongshore wind stress and open-ocean forcings) on the varying parameters. For example, the spatial scale of both forcings and the slope of shelf have the same effect in determining the coastal sea level; namely, larger scale of the forcings and/or gentler slope would lead to larger amplitude of coastal sea level and/or larger penetration of interior sea level. The bottom friction, however, would exert the opposite effect, i.e., smaller friction would lead to larger amplitude of coastal sea level induced by local wind, but would lead to less transmission of the open-ocean signals onto the coast.

The aforementioned findings are obtained from the linearized, ideal model forced by simplified forcings. In the next section, we will apply this modified ATW model to examine the coastal sea level at the west coasts of North Pacific (or the ECS) and North Atlantic, considering more realistic local and remote forcings. In particular, resolving the transmission of the open-ocean forcing is essential in the ultimate reconstruction of sea level at the coast. We will start from the application to the ECS.

4. Results

4.1. Sea Level at the Open-Ocean Boundary

The classic wind-driven ocean circulation theory suggests that the equatorward transport in the subtropical gyre interior (Sverdrup, 1947) is balanced by the poleward transport of the western boundary current. The western boundary current was studied in a basin with a flat bottom and vertical sidewalls, forced by winds and dissipated either by the bottom friction parameterized by a linear drag (Stommel, 1948) or by the lateral friction parameterized by a form of biharmonic viscosity (Munk, 1950). For the sea level at the west wall of the western boundary current (x_W in Figure 1), Godfrey (1975) yielded a diagnostic relation for the distribution of thermocline depth (and hence sea surface height) along the wall, which includes the direct effect of internal Rossby waves. In a beta-planed, steady, and nondivergent system, Pedlosky (1996) proposed that coastal sea level along the wall is determined by an ocean-interior stream function. More recently, Minobe et al. (2017) further extended these works and showed that the linkage between the sea level at the vertical sidewalls (i.e., the sea level at the west wall of the western boundary current) and sea level at the western end of ocean interior can be quantified in a linear, reduced gravity model as

$$\eta\left[x_W(y),\, y,\, t\right] = \frac{f(y)}{f\left(y_P\right)}\eta\left[x_W\left(y_P\right),\, y_P,\, t\right] + f(y)\int_y^{y_P}\frac{\beta}{f^2}\eta\left[x_I\left(y'\right),\, y',\, t\right]dy' \tag{5}$$

where x_W and x_I are the zonal positions of the west wall of western boundary current (i.e., western boundary layer) and the western end of ocean interior, respectively (Figure 1), y and y_P are the meridional position of interest and a reference site at a higher latitude, $f(y)$ is Coriolis parameter and $\beta = df/dy$ is the meridional derivative of the Coriolis parameter. Equation 5 means that sea level along the west wall of the western boundary layer (x_W in Figure 1) at a lower latitude is given by the sum of sea level at a higher latitude and the contribution of the incoming long Rossby waves between the two latitudes. The Coriolis parameter $f(y)$ appears in both terms on the right-hand side, indicating that sea level reduces its amplitude equatorward in proportion to f. The physical interpretation is that the mass flux into the western boundary layer due to incident Rossby waves from the ocean

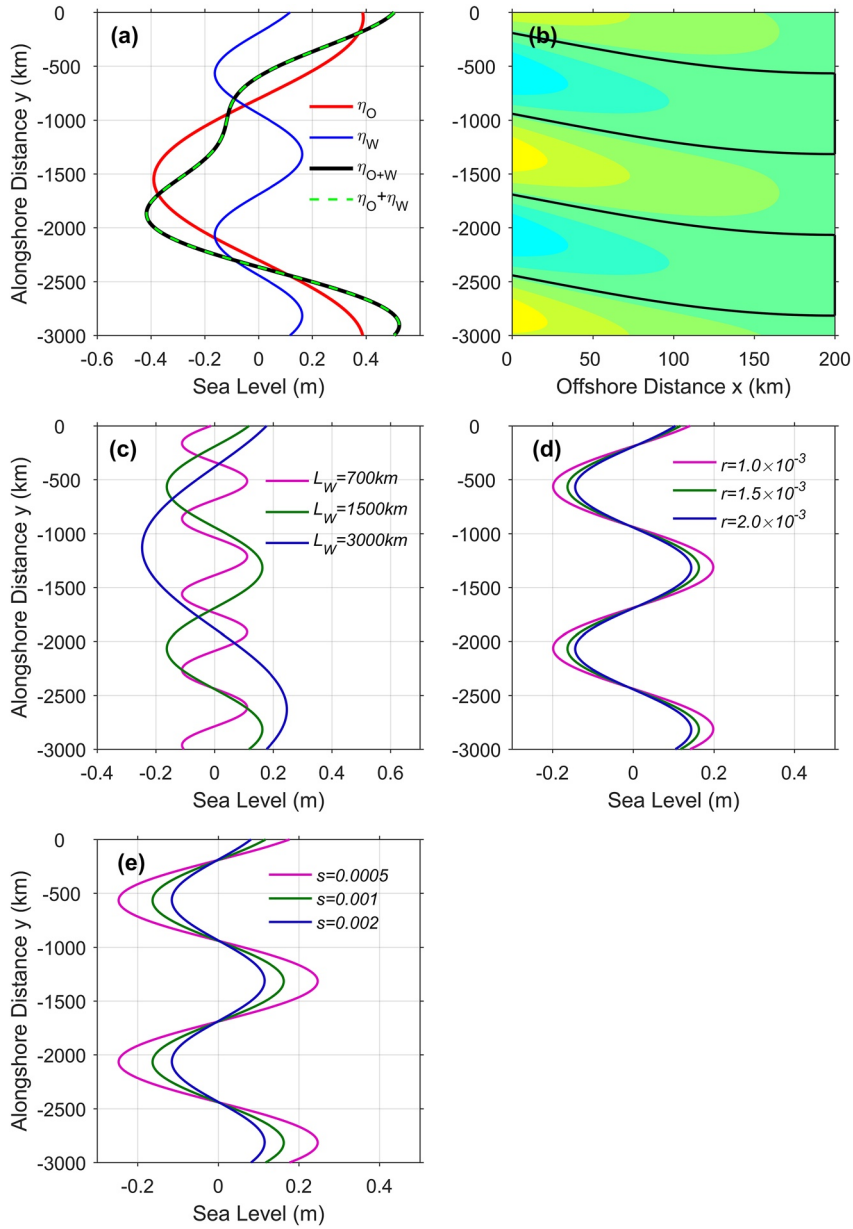

Figure 5. (a) Coastal sea level derived from the model experiment that is forced by wind stress only (η_W), by open-ocean boundary only (η_O), and by both the wind stress and open-ocean forcing (η_{O+W}). The dotted green line is the sum of η_O and η_W. (b) Sea level distribution from an experiment that is forced only by local wind stress. Coastal sea level from three sensitivity experiments (forced by wind stress only) with varying (c) wavelength of the alongshore wind, (d) friction coefficient, and (e) slope of the shelf. A complete list of model parameters for all the experiments in this figure is summarized in Table 1. The alongshore distance is intentionally extended to 3,000 km to view more detailed features of coastal sea level.

interior must be carried equatorward by coastal trapped waves (Hughes et al., 2019). Therefore, we will use Equation 5 to calculate sea level at the west wall (x_W) of the Kuroshio in the ECS and regard it as the open-ocean boundary condition for our model on the ECS shelf. Notice, however, that the derivation in Minobe et al. (2017) assumed a flat bottom at the western boundary layer and a vertical sidewall at its western edge (x_W in Figure 1). The vertical sidewall solution is a special limit case for the more general problem that includes sloping bathymetry on the continental shelf/slope (Wise et al., 2018). The result of Minobe et al. (2017) applied here provides the maximum sea level signals at the west wall of the western boundary layer (x_W in Figure 1). Namely, the vertical sidewall assumes almost no insulation of the sea level of ocean interior.

Table 1
Model Parameters for All Sensitivity Experiments in Figure 5

Cases	Slope s	Friction coefficient r (m s^{-1})	Wind stress $F = F_1\sin(\frac{2\pi}{L_w}y)$ (m^2 s^{-2})	Open-ocean forcing $\eta_O = \eta_1\sin(\frac{2\pi}{L_O}y)$
A1	0.001	1.5×10^{-3}	$F_1 = 0$	$\eta_1 = 1$, $L_O = 3{,}000$ km
A2	0.001	1.5×10^{-3}	$F_1 = -0.4 \times 10^{-3}$, $L_w = 1{,}500$ km	$\eta_1 = 0$
A3	0.001	1.5×10^{-3}	$F_1 = -0.4 \times 10^{-3}$, $L_w = 1{,}500$ km	$\eta_1 = 1$, $L_O = 3{,}000$ km
B	0.001	1.5×10^{-3}	$F_1 = -0.4 \times 10^{-3}$, $L_w = 1{,}500$ km	$\eta_1 = 0$
C1	0.001	1.5×10^{-3}	$F_1 = -0.4 \times 10^{-3}$, $L_w = 700$ km	$\eta_1 = 0$
C2	0.001	1.5×10^{-3}	$F_1 = -0.4 \times 10^{-3}$, $L_w = 1{,}500$ km	$\eta_1 = 0$
C3	0.001	1.5×10^{-3}	$F_1 = -0.4 \times 10^{-3}$, $L_w = 3{,}000$ km	$\eta_1 = 0$
D1	0.001	1.0×10^{-3}	$F_1 = -0.4 \times 10^{-3}$, $L_w = 1{,}500$ km	$\eta_1 = 0$
D2	0.001	1.5×10^{-3}	$F_1 = -0.4 \times 10^{-3}$, $L_w = 1{,}500$ km	$\eta_1 = 0$
D3	0.001	2.0×10^{-3}	$F_1 = -0.4 \times 10^{-3}$, $L_w = 1{,}500$ km	$\eta_1 = 0$
E1	0.0005	1.5×10^{-3}	$F_1 = -0.4 \times 10^{-3}$, $L_w = 1{,}500$ km	$\eta_1 = 0$
E2	0.001	1.5×10^{-3}	$F_1 = -0.4 \times 10^{-3}$, $L_w = 1{,}500$ km	$\eta_1 = 0$
E3	0.002	1.5×10^{-3}	$F_1 = -0.4 \times 10^{-3}$, $L_w = 1{,}500$ km	$\eta_1 = 0$

Note. The Coriolis parameter is $f = 10^{-4}$ s^{-1} and gravitational acceleration is $g = 9.8$ m s^{-2}. F_1 and η_1 are the amplitude of the wind stress and open-ocean signals, respectively.

We now turn to sea level calculation in the ocean basin. Vivier et al. (1999) estimated the contributions of sea level accounted for by various processes in the Pacific. They pointed out that in the subtropical North Pacific, the baroclinic sea level component (via westward propagating Rossby waves) overwhelms the barotropic component (estimated by Sverdrup balance); in the subarctic region, however, the Sverdrup dynamics dominate the sea level variation after removing the steric component (Isoguchi & Kawamura, 2006; Stammer, 1997). Here, we consider both the baroclinic and barotropic adjustment processes of sea level changes in the ocean interior. The large-scale, baroclinic sea level response to surface wind forcing is calculated by (Qiu, 2003)

$$h_{bc}(x,y,t) = h_{bc}\left(x_e, y, t + \frac{x - x_e}{c_R}\right) + \frac{g'}{\rho_0 g f c_R}\int_{x_e}^{x} \nabla \times \boldsymbol{\tau}\left(x', y, t + \frac{x - x'}{c_R}\right) dx' \tag{6}$$

where h_{bc} is the sea level of interest, g' is the reduced gravity, x_e is the longitudinal location of the eastern boundary, ρ_0 is the reference density, c_R is the phase speed of the baroclinic Rossby waves depending on the latitude, $\nabla \times \boldsymbol{\tau}$ is the wind stress curl, and sea level along the eastern boundary $h_{bc}(x_e, y, t)$ is assumed to be zero. Fu and Qiu (2002) suggested that the forcing along the eastern boundary is of little importance in regulating the large-scale sea level signals in the interior midlatitude North Pacific Ocean. The barotropic sea level component is calculated via the Sverdrup balance as (Qiu, 2002)

$$\frac{\partial h_{bt}}{\partial x} = \frac{f_0 \nabla \times \boldsymbol{\tau}}{\rho_0 g \beta H} \tag{7}$$

where h_{bt} denotes the part of sea level changes due to barotropic processes, β is the meridional gradient of f, H is the mean water depth, and f_0 is the Coriolis parameter at the reference latitude. Zonal integration of this equation from the eastern boundary leads to the interior solution. The sum of the baroclinic and barotropic components, which agrees well with the observed sea level from satellite altimeter at the corresponding latitudes (figure not shown), gives the sea level at the western end of ocean interior, and will be used as the sea level of ocean interior (x_I in Figure 1) in the second term on the right-hand side of Equation 5.

Sea level along the west wall (x_W in Figure 1) of the western boundary current (i.e., Kuroshio) is then calculated according to Equation 5 using realistic wind forcing in the North Pacific. It is evident that there is a long-standing northward drop for sea level at the west wall of the Kuroshio (Figure 6a), which is set up by the wind-driven anticyclonic gyre in the ocean interior. The difference of annual mean sea level between 21.5°N and 30.5°N is 0.16 m, yielding an averaged sea level tilt of about −1.6 cm/100 km. Steeper tilt occurs in winter that typically exceeds

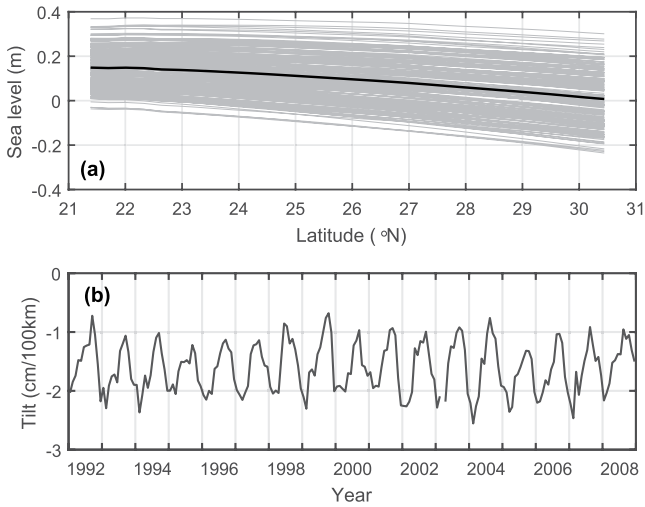

Figure 6. (a) Sea level at the west wall of the Kuroshio estimated by Equation 5. The gray lines indicate the monthly profiles of open-ocean signal for the period of 1992–2008, and the black line is the averaged profile which is used as the open-ocean boundary condition for the modified arrested topographic wave (ATW) model. (b) Monthly tilt of sea level at the west wall of the Kuroshio (gray lines in (a)).

−2.0 cm/100 km (Figure 6b). If this northward sea level drop at the outer edge of the ECS shelf (i.e., the west wall of the Kuroshio) directly projects to the coast, it may explain the overall northward drop in the Chinese coastal sea level, as well as its evident seasonality documented in Lin et al. (2021). Therefore, we consider an alongshore pressure gradient as the open-ocean boundary condition to represent the oceanic influence in our linear, modified ATW model. Given the monotonic sea level drop toward north, we adopt a quarter of the sinusoidal form of sea level $\eta(L_x, y) = \eta_1 \sin(2\pi k y)$ at the offshore boundary, which has an alongshore wavelength of $1/k = 6{,}000$ km. This is similar to the pressure gradient along the western end of ocean interior set up by the subtropical and subpolar basin circulations (Huang, 2010).

4.2. Relative Contributions of Open-Ocean Signals and Alongshore Wind Stress

As aforementioned, the open-ocean signals diffuse effectively shore-ward to the coast with enhanced bottom friction (Wise et al., 2020; Wu, 2021). It is thus necessary to prescribe accurate bottom friction in the modified ATW model for our study region. Here, the cross-shelf slope s has been fixed as $s = 0.001$, mimicking the topography of the ECS continental shelf. To this end, we conduct several additional experiments with different friction coefficients (Figure 7a). The model is forced both by (a) the open-ocean forcing, with an averaged tilt of sea level of −1.6 cm/100 km (Figure 6a; black line) corresponding to an amplitude of $\eta_1 = 0.24$ m over an alongshore distance of $L_y = 1{,}500$ km, and (b) the local wind forcing, with a constant alongshore (kinematic) wind stress $F = -0.2 \times 10^{-3}$ m^2 s^{-2} given the realistic annual mean wind stress over the coastal zone of ECS. It is shown that the tilt of coastal sea level becomes steeper with increasing friction (Figure 7a). The estimated tilt from tide-gauge observations is about −1.4 cm/100 km along the coast of ECS (Lin et al., 2021), which corresponds to a friction coefficient $r = 14 \times 10^{-4}$ m s^{-1} (the red star in Figure 7a).

With this prescribed bottom friction $r = 14 \times 10^{-4}$ m s^{-1} and the slope of shelf $s = 0.001$, we first conduct an experiment in which the model is forced only by the open-boundary condition (Figure 7b), which has a sea level tilt of −1.6 cm/100 km (Figure 6a). This experiment allows us to explore the penetration ratio of open-ocean signals. The cross-shelf sea level along the characteristic lines indicates that the open-ocean magnitude reduces by $(0.24 - 0.15)/0.24 = 37\%$ (see solid and dashed lines in Figure 7d), giving a penetration ratio of $0.15/0.24 = 0.63$. To further investigate the contribution of local wind forcing, we conduct another experiment in which the model is forced by both the open-ocean forcing and the alongshore wind stress (Figure 7c). Given that the magnitude of the penetrated open-ocean signals is 0.15 m, the contribution of sea level induced by the local alongshore wind stress is $(0.44 - 0.15)/0.44 = 66\%$ (dot-dashed line in Figure 7d). Therefore, in the linear regime, we are able to infer that the contributions of open-ocean signals and alongshore wind stress account for 34% and 66% of the coastal sea level variance, respectively, under the prescribed model parameters mimicking the ECS.

4.3. Coastal Sea Level Reconstruction

Up to now, we have managed to (a) calculate sea level at the western end of ocean interior (x_I in Figure 1) by integrating the oceanic barotropic and baroclinic responses to large-scale wind forcing in the North Pacific basin, (b) calculate sea level at the west wall of the Kuroshio (x_W in Figure 1) using the above interior information following Minobe et al. (2017), and finally (c) calculate the penetrated sea level at the coast of ECS based on the modified ATW model using sea level from (b) as the boundary condition and the inferred penetrated ratio. In this way, we are able to estimate coastal sea level induced by the open-ocean forcing using simply the remote wind forcing. Adding the component induced by the local alongshore wind stress, we will be able to reconstruct sea level at the coast.

We choose the Kanmen tide-gauge station (Figure 2) as an example to do the sea level reconstruction. This station is situated roughly in the middle of ECS which is in fact a suitable location, considering the equatorward

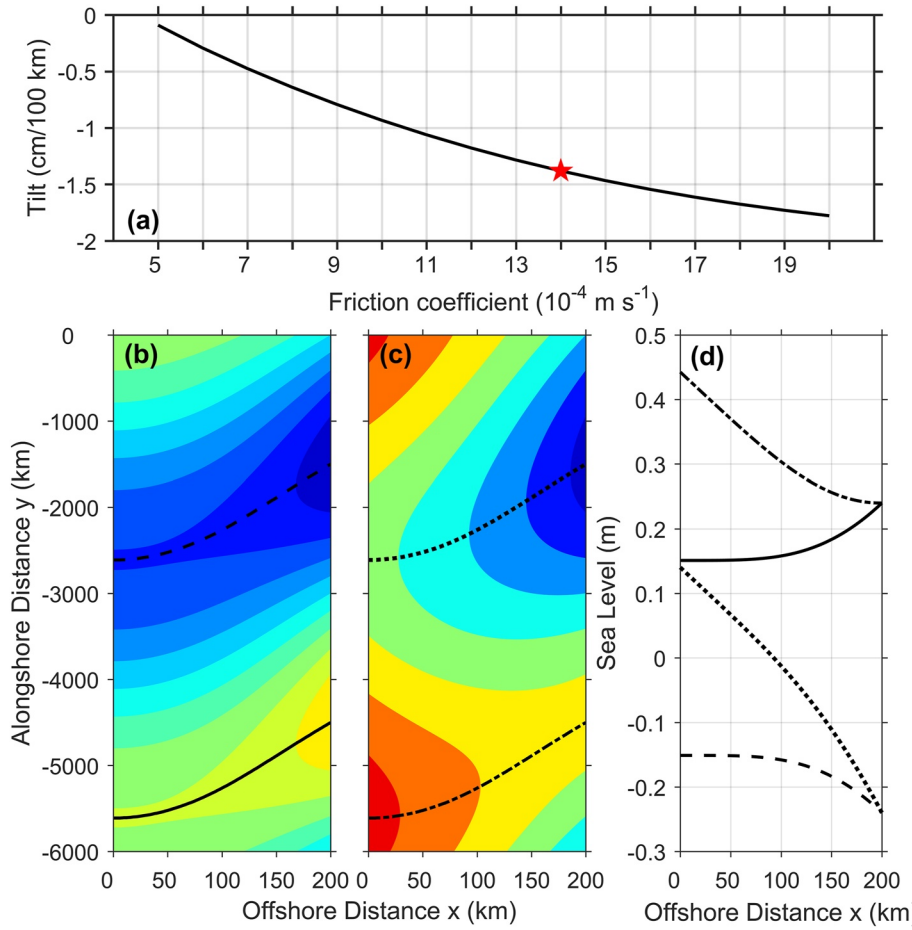

Figure 7. (a) The coastal sea level tilt as a function of bottom friction coefficient. The friction coefficients range from 5×10^{-4} m s^{-1} to 20×10^{-4} m s^{-1}, with an interval of 1×10^{-4} m s^{-1}. Simulated sea level on the shelf from the linear model which is (b) forced only by the open-ocean forcing and (c) forced by both the open-ocean forcing and alongshore wind stress. The friction coefficient is $r = 14 \times 10^{-4}$ m s^{-1} for both runs, and the slope of shelf is $s = 0.001$. The different black lines indicate the characteristic lines of propagation. The color scales in (b) and (c) both range from −0.3 to 0.5 m. (d) Cross-shelf profiles of the sea level along the characteristic lines (shown in corresponding line styles as in panels (b) and (c)).

displacement of the open-ocean signals and allowing also for influence from higher latitudes via coastal trapped waves. The observed time series of monthly sea level anomalies from Kanmen tide gauge (Figure 8a, black line; η_{Obs}) exhibits a clear seasonal cycle with peaks in autumn and troughs in spring. The inverse barometer effect was removed from the tide-gauge measurements, whereas the steric-height variation was retained.

In winter, the ECS is predominantly forced by northeasterly winds. This wind pattern is favorable for the pile up of water resulting in a poleward alongshore pressure gradient force that serves as one of the main driving forces for the observed sea level tilt. Lin et al. (2021) suggested that the wintertime sea level along the coast of the Chinese mainland is well predicted by the ATW model. We thus examine the effect of alongshore wind stress on seasonal sea level variations along the west coast of ECS using the ATW model (Csanady, 1978; Hickey & Pola, 1983). Csanady (1978) presented a solution for the sea level forced by a piecewise wind stress in a coastal region, ignoring the open-ocean forcing (i.e., $\eta = 0$ at $x \to \infty$)

$$\eta(y) = -\frac{1.8 f \tau_0}{rg} \left\{(-Ky)^{1/2} - [K(Y-y)]^{1/2}\right\} \tag{8}$$

where the wind stress is prescribed for $Y > y > 0$ and zero elsewhere, $K = r/(fs)$ with the notations the same as above. This equation implies that the sea level at a targeted latitude is the integral of sea level induced by the piecewise alongshore wind stress over the integral route from a reference latitude to the targeted latitude. Since

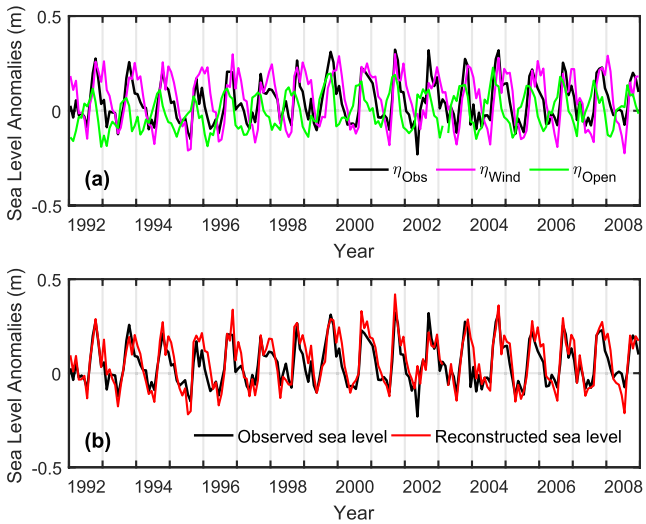

Figure 8. (a) Observed monthly time series of sea level from tide-gauge measurements (black line), sea level induced by local alongshore wind stress (purple line) and open-ocean sea level (green line). The time-averaged sea level has been removed for each time series. (b) Comparison of the observed sea level (black line) and the reconstructed sea level estimated by Equation 9 (red line).

the annual mean prevailing wind is almost perpendicular to the coastline north of ~35°N (Lin et al., 2021), the reference latitude is taken to be 35°N as the starting point of integral route. According to Equation 8, the calculated sea level component induced by realistic alongshore wind (Figure 8a, η_{Wind}; purple line) indeed accounts for a large proportion of the observed sea level variation. The peak of η_{Wind} (November to January) corresponds to the periods with strong winds as expected, and the phase difference between η_{Obs} and η_{Wind} is likely caused by other dynamical processes. Based on Equation 5, the sea level component induced by the open-ocean forcing is calculated (Figure 8a, η_{Open}; green line) using realistic wind stress. Here, we choose Nisinoomote tide-gauge station (Figure 2) as the reference site at the higher latitude, and the sea level from this tide gauge (the IB effect removed) is used to estimate the contribution of signals from poleward via coastal trapped waves (i.e., the first term on the right-hand side of Equation 5). The amplitude of η_{Open} is generally weaker than that of η_{Wind} with the phase of η_{Open} slightly leading, particularly at troughs.

Recalling that the penetration ratio of open-ocean signals to the coast is 0.63, we are able to reconstruct the coastal sea level (η_{Recon}) in the linear framework as follows:

$$\eta_{Recon} = \eta_{Wind} + 0.63 \times \eta_{Open} \quad (9)$$

The red line in Figure 8b depicts the reconstructed coastal sea level from Equation 9, which fits fairly well with the observed sea level from tide-gauge measurements (η_{Obs}; black line). The correlation coefficient between η_{Recon} and η_{Obs} is $R = 0.91$ ($p < 0.05$). The close agreement demonstrates that it is indeed possible to reconstruct/forecast coastal sea level using solely the local and remote wind forcings, at least at the seasonal time scale.

It is worthwhile to note that the above reconstruction assumes that the sea level components induced by the local and remote forcings could be added together linearly. We recognize that there might be nonlinear interactions between different components, in particular for the ones induced by high-frequency processes such as wind waves, meteotsunamis, storm surges, etc. (LeBlond & Mysak, 1978; Monserrat et al., 2006). In the present study, we focus on the lower-frequency variability of coastal sea level, which, to a large extent, satisfies the linear regime assumption. The monthly sea-level time series has already filtered out high-frequency signals mentioned above.

4.4. Application to the West Coast of North Atlantic

The sea level reconstruction at the west coast of ECS has shown promising results. What is more interesting is whether the reconstruction procedure, built on the "basin-to-coast" dynamical linkage proposed in this study, could be applied to the west coasts of other ocean basins. According to the above calculations, the key is to figure out the relative contributions of open-ocean signals (or the penetration of open-ocean signals) and local alongshore wind stress. We now try to reconstruct the sea level at the west coast of North Atlantic to test the validity of the dynamical linkage. The dynamical settings between the western North Atlantic and North Pacific bear important similarities, e.g., both basins contain the most prominent western boundary currents (Figure 2) that flow over continental slope separating the deep ocean basin and shallow shelf.

We first consider the role of the local wind stress. Although the wind stress is strong in winter, the wind direction is mostly perpendicular to the coastline (Figure 9a). The wind stress gets significantly weakened in spring and continues to be perpendicular to the coast, especially north of 35°N (Figure 9b). In summer, the wind stress is mostly alongshore but its magnitude is the weakest among four seasons, with a mean value of 0.02 Pa (Figure 9c). In autumn, wind stress returns to be approximately normal to the shore north of 35°N (Figure 9d), but is roughly alongshore (northeasterlies) south of 35°N. It becomes clear that the wind direction (especially north of 35°N) is mostly perpendicular to the coast over the North Atlantic shelf (i.e., the alongshore component of wind stress is weak), indicating that the local wind forcing is likely to be insignificant for the coastal sea level variability. In this case, we can ignore the sea level component induced by the local wind stress using the ATW model

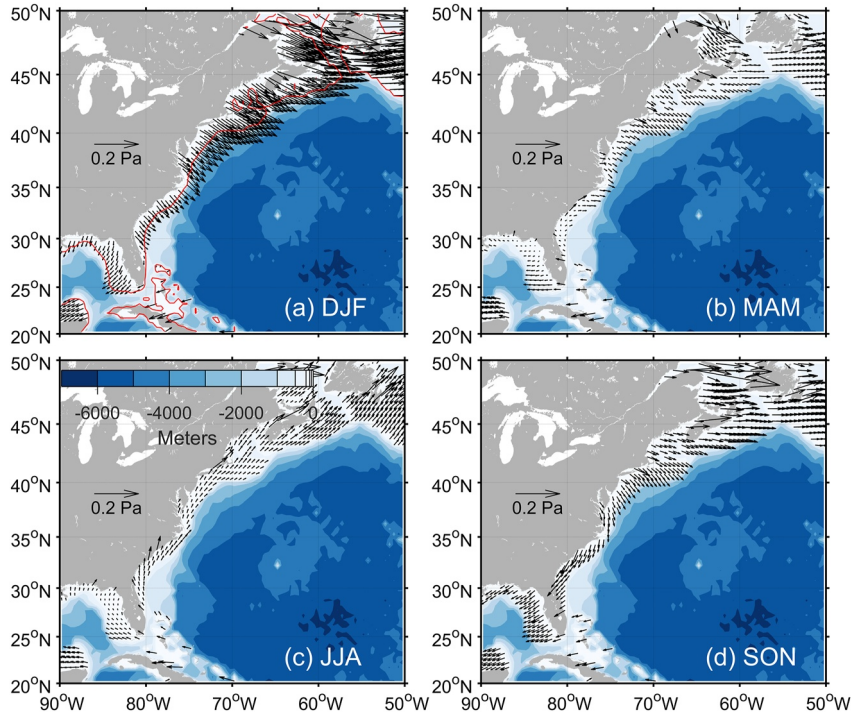

Figure 9. Spatial distributions of wind stress from NCEP CFSR (1979–2010) in different seasons over the western shelf of North Atlantic. The background color is the bathymetry (in m) and the red lines in (a) denote the 200-m isobaths.

(Csanady, 1978). Then the reconstruction equation (Equation 9: $\eta_{\mathrm{Recon}} = \eta_{\mathrm{Wind}} + 0.63 \times \eta_{\mathrm{Open}}$) simply reduces to $\eta_{\mathrm{Recon}} = \alpha \times \eta_{\mathrm{Open}}$, where α is the penetration ratio of open-ocean signals in the North Atlantic basin.

Now we consider the open-ocean signals and their penetration ratio (α). The sea level of ocean interior (x_I in Figure 1) is calculated by Equations 6 and 7 (Qiu, 2002, 2003) to account for the westward-propagating baroclinic and barotropic Rossby waves driven by open-ocean wind stress curl in the North Atlantic. To account for the contribution of coastal trapped waves from poleward, we use altimeter-based sea level anomaly data at a higher-latitude referenced site, because there are no available tide-gauge measurements along the west wall of Gulf Stream (x_W in Figure 1). The open-ocean sea level (x_W in Figure 1) can subsequently be estimated according to Equation 5 (Minobe et al., 2017). To infer the penetration ratio of open-ocean signals in the western North Atlantic, we design and conduct a series of experiments using the modified ATW model that is forced only by the open-ocean forcing, similar to the implementations in the ECS. We adopt a quarter of the sinusoidal form of sea level $\eta(L_x, y) = \eta_1 \sin(2\pi k y)$ at the offshore boundary, which has an alongshore wavelength of $1/k = 6{,}000$ km. With other model parameters set mimicking the North Atlantic shelf, the sensitivity experiments regarding on bottom friction coefficient r and the slope of shelf s indicate that the penetration rate (α) ranges between 0.50 and 0.96 (Figure 10).

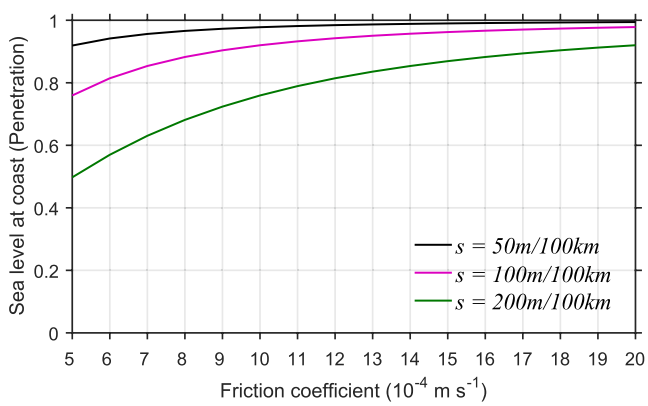

Figure 10. Sea level at the west coast of North Atlantic (the penetration rate of open-ocean signals) as a function of the bottom friction coefficient at different slopes of shelf (s). The experiments are forced only by the open-ocean forcing.

Finally, we choose two tide gauges (red dots in Figure 11a) at the east coast of North American as examples to do the sea level reconstruction. We remove the IB effect from the observed sea level but retain the steric-height variations, as we did in Figure 8. Figures 11b and 11c exhibit evident seasonality in the observed sea-level time series (η_{Obs}; black lines). With the simplified reconstructed equation ($\eta_{\mathrm{Recon}} = \alpha \times \eta_{\mathrm{Open}}$) and the mean penetration rate in the case of $s = 200$ m/100 km ($\alpha = 0.78$), the reconstructed sea levels (red lines in Figures 11b and 11c) show fairly good agreement with the observations (the correlations $R = 0.61$ and $R = 0.59$; $p < 0.05$). The successful application of

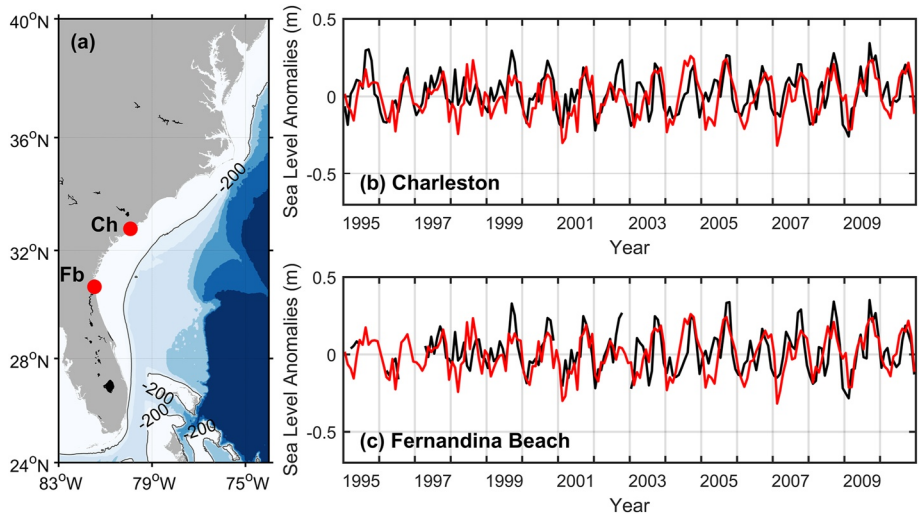

Figure 11. (a) Location of the tide gauges (red dots with initials of the station names). The gray lines indicate the 200-m isobaths. Ch and Fb denote the Charleston tide-gauge station and Fernandina Beach tide-gauge station, respectively. Comparison of the observed sea level (black lines) and the reconstructed sea level (red lines) at Charleston (b) and Fernandina Beach (c).

sea level reconstruction at the west coast of North Atlantic verifies the reliability of the "basin-to-coast" dynamical linkage proposed in the present study.

5. Conclusions and Discussion

This study dedicates to dynamically reconstruct sea level at the coast based on the local wind forcing and remote open-ocean signals. Estimate of sea level component induced by the local wind is based on the ATW model of Csanady (1978). Estimate of sea level component induced by the remote open-ocean forcing is grounded on the "basin-to-coast" dynamical linkage framework that requires understanding and quantification of a series of dynamic processes, including the barotropic response via Sverdrup dynamics, the baroclinic response via Rossby waves, the transmission processes across the western boundary current/continental slope, and ultimately the penetrating processes across the shelf to the coast. We have shown in the present study that the low-frequency (not shorter than seasonal) variability of coastal sea level could be well reconstructed in the linear framework given realistic local alongshore wind and the large-scale wind forcing in the ocean basin interior. The success in the sea level reconstruction at the west coasts of North Pacific and North Atlantic proves the reliability of the "basin-to-coast" dynamical linkage we build in this study. The reconstruction idea and specific calculations could be readily applied to other coasts around the global ocean.

We use a modified ATW model to examine the distribution of sea level over the continental shelf. This model demonstrates that sea level signal from ocean interior can penetrate to the coast with an equatorward displacement and an attenuation in its amplitude. The wind stress would not affect the transmission of open-ocean signals (in the linear regime), but will significantly influence the local variations of coastal sea level and hence its alongshore tilt. The modeled coastal sea level is sensitive to the representation of bottom friction, the slope of shelf and the spatial scale of open-ocean signals. Overall, larger-scale signals at the offshore boundary would result in greater penetration of interior sea level signal to the coast, and larger-scale local wind stress at the coastal boundary would lead to greater amplitude of sea level at the coast. Larger bottom friction is more likely to break the conservation of potential vorticity and to increase the penetration across isobaths with less equatorward displacement and less attenuation in amplitude; but larger friction would reduce the magnitude of the coastal sea level component caused by alongshore wind stress. Less steep slope of the shelf favors greater penetration of the interior signals, and the coastal sea level also responses more effectively to the alongshore wind stress under gentler slope of shelf.

We first apply this modified ATW model to the ECS with the model parameters (e.g., slope of shelf, friction coefficient, open-ocean condition, etc.) being set on the basis of realistic features of the ECS. For example, the slope

of the wedge-shaped shelf is set to be $dh/dx = s = 0.001$ considering the ECS bathymetric feature (depth changes from 0 to 200 m over a shelf width of 200 km), the annual mean alongshore wind stress from NCEP/CFSR is set as the boundary condition at the coast, and the sea level estimated from Equation 5 is set as the open boundary condition. The friction coefficient ($r = 14 \times 10^{-4}$ m s^{-1}) is chosen according to the observed alongshore sea level gradient (−1.4 cm/100 km) at the ECS coast. With these model parameters, we evaluate that the interior sea level signals will be attenuated by 37% when reaching the coast, namely 63% of the deep-ocean signal manages to penetrate across the shelf, and this part of sea level component accounts for 34% of the total sea level at the coast. The remaining 66% component is attributed to the local alongshore wind stress. Both components can be calculated directly from the wind stress field. Ultimately, we are able to estimate the sea level along the west coast of ECS in the linear framework using all these components induced by differing dynamic processes. The reconstructed coastal sea level highly resembles the observed sea level from tide-gauge measurements ($R = 0.91$; $p < 0.05$). Further, we apply the model to reconstruct sea level at the west coast of North Atlantic with the model parameters set according to the realistic features of western North Atlantic shelf. It is found that the local wind stress plays a limited role in the coastal sea level variability and is thus ignored. After a set of model sensitivities, we obtain the mean penetration ratio (i.e., 0.78) of open-ocean signals; using this ratio, we can reconstruct sea level at the west coast of North Atlantic and again find fairly good agreement with tide-gauge observations ($R = 0.61$ and 0.59). The success in reconstructing sea level at the west coasts of both North Pacific and North Atlantic demonstrates the reliability and genericity of the dynamical linkage framework proposed in this study.

There are two points that worth to be mentioned.

i. For the west coasts of ocean basins, coastal sea level is reconstructed by quantifying the contributions of (a) open-ocean forcing via the "basin-to-coast" dynamical linkage framework and (b) the local wind forcing via the traditional ATW model. For the east coasts, it is in fact easier to reconstruct coastal sea level by simply quantifying the local wind forcing on the shelf using the traditional ATW model; so coastal sea level reconstruction at the east coasts could be viewed as a simpler case of the dynamical framework. We choose a tide-gauge station (Yakutat) located at the east coast of Pacific Ocean as an example to do the sea level reconstruction only considering the alongshore wind stress, and the reconstructed sea level is in close agreement with the observed sea level (figure not shown). It is thus promising to apply the proposed rationale in this study to achieve a better estimate/forecast of the coastal sea level at other coasts of the global ocean.
ii. In order to check whether the good agreement between the reconstructed and observed sea levels is due primarily to the inclusion of seasonal cycles, we further compare the deseasonalized reconstructed and observed sea levels (figure not shown). Interestingly, at Kanmen station situated at the Chinese coast, the reconstructed sea level shows a fairly good agreement with the observations at the interannual time scale ($R = 0.66$; $p < 0.05$), whereas the agreement at Charleston station degrades substantially ($R = 0.13$; $p < 0.05$). In other words, following the dynamical framework proposed in this study, the reconstructed sea level seems to be able to capture both the seasonal and interannual variability of observed sea level along the west coast of North Pacific, but can only capture the seasonal variation of observations along the west coast of North Atlantic.

Although the reconstruction works well, the *f*-plane approximation of the linear model could be problematic if the meridional extent of the shelf is large, and it remains to be investigated to what extent the results from this model might be altered if the variation of ambient potential vorticity (induced mainly by planetary β effect) is considered (Wise et al., 2018; Wu, 2021). The impact of an inclined shelf/slope instead of a vertical sidewall at the west edge of the western boundary layer also needs to be further investigated when quantifying the transmission processes across the western boundary currents. As mentioned above, the impact of higher-frequency dynamics on the short-term coastal variability has been neglected in this study, and the reconstruction of coastal sea level including this frequency band is more challenging. The linear model used here has been intentionally simple, with the aim of building a neat, seamless dynamic linkage from the ocean basin to the coast.

In addition, we have excluded the influence of freshwater influx (e.g., river discharge, precipitation) at the shore, which could also significantly impact the variations of coastal sea level via mass and/or steric contributions (Durand et al., 2019; Piecuch & Wadehra, 2020; Piecuch et al., 2018). For example, Piecuch et al. (2018) suggested that the rive discharge is significantly correlated to sea-level changes on the United States Atlantic and Gulf coasts. Chandanpurkar et al. (2022) predicted nonseasonal river-discharge impact on sea level variability using the simplified theory proposed by Piecuch et al. (2018). Similarly, precipitation and buoyancy forcings

could also play roles in the variations of coastal sea level (Lee et al., 2019; Wang et al., 2022). The impacts of the above-mentioned processes/settings (including the β effect, freshwater influx, momentum advection, time dependence, and the vertical/inclined sidewall) on the detailed sea level adjustment will be investigated in a more sophisticated numerical model in the next step.

Data Availability Statement

Tide-gauge observations used in the paper are obtained from the Permanent Service for Mean Sea Level (PSMSL; https://www.psmsl.org/). The surface atmospheric pressure is collected from the climatological monthly means of National Centers for Environmental Prediction/National Center for Atmospheric Research (NCEP/NCAR; https://psl.noaa.gov/data/gridded/data.ncep.reanalysis.html). The wind stress is obtained from the NCEP Climate Forecast System Reanalysis (NCEP/CFSR; https://rda.ucar.edu/datasets/ds093.2/). The software associated with this manuscript for the ATW model is provided on GitHub https://github.com/Linwq0412/ATW-model.

Acknowledgments
This study was supported by the National Natural Science Foundation of China (91958203, 42076013, 91858201, 41730533, 41890801) and the Natural Science Foundation of Fujian Province of China (2019J05009). The authors would like to appreciate two anonymous reviewers who provided useful comments that have help improve an early version of the manuscript.

References

Chandanpurkar, H. A., Lee, T., Wang, X., Zhang, H., Fournier, S., Fenty, I., et al. (2022). Influence of nonseasonal river discharge on sea surface salinity and height. *Journal of Advances in Modeling Earth Systems*, *14*, e2021MS002715. https://doi.org/10.1029/2021MS002715

Csanady, G. T. (1978). The arrested topographic wave. *Journal of Physical Oceanography*, *8*(1), 47–62. https://doi.org/10.1175/1520-0485(1978)008<0047:tatw>2.0.co;2

Csanady, G. T. (1982). Circulation in the coastal ocean. *Advances in Geophysics*, *23*, 101–183. https://doi.org/10.1007/978-94-017-1041-1

Durand, F., Piecuch, C. G., Becker, M., Papa, F., Raju, S. V., Khan, J. U., & Ponte, R. M. (2019). Impact of continental freshwater runoff on coastal sea level. *Surveys in Geophysics*, *40*, 1437–1466. https://doi.org/10.1007/s10712-019-09536-w

Fu, L. L., & Qiu, B. (2002). Low-frequency variability of the North Pacific Ocean: The roles of boundary- and wind-driven baroclinic Rossby waves. *Journal of Geophysical Research*, *107*(C12), 3220–3221. https://doi.org/10.1029/2001JC001131

Godfrey, J. S. (1975). On ocean spindown I: A linear experiment. *Journal of Physical Oceanography*, *5*, 399–409. https://doi.org/10.1175/1520-0485(1975)005<0399:oosial>2.0.co;2

Hickey, B. M., & Pola, N. E. (1983). The seasonal alongshore pressure gradient on the west coast of the United States. *Journal of Geophysical Research*, *88*(C12), 7623–7633. https://doi.org/10.1029/JC088iC12p07623

Higginson, S., Thompson, K. R., Woodworth, P. L., & Hughes, C. W. (2015). The tilt of mean sea level along the east coast of North America. *Geophysical Research Letters*, *42*, 1471–1479. https://doi.org/10.1002/2015GL063186

Holgate, S. J., Matthews, A., Woodworth, P. L., Rickards, L. J., Tamisiea, M. E., Bradshaw, E., et al. (2013). New data systems and products at the permanent service for mean sea level. *Journal of Coastal Research*, *29*(3), 493–504. https://doi.org/10.2112/JCOASTRES-D-12-00175.1

Huang, R. X. (2010). *Ocean circulation: Wind-driven and thermohaline processes* (pp. 273–276). Cambridge University Press.

Hughes, C. W., Fukumori, I., Griffies, S. M., Huthnance, J. M., Minobe, S., Spence, P., et al. (2019). Sea level and the role of coastal trapped waves in mediating the influence of the open ocean on the coast. *Surveys in Geophysics*, *40*, 1467–1492. https://doi.org/10.1007/s10712-019-09535-x

Hughes, C. W., Williams, J., Blaker, A., Coward, A., & Stepanov, V. (2018). A window on the deep ocean: The special value of ocean bottom pressure for monitoring the large-scale, deep-ocean circulation. *Progress in Oceanography*, *161*, 19–46. https://doi.org/10.1016/j.pocean.2018.01.011

Huthnance, J. M. (1987). Along-shelf evolution and sea levels across the continental slope. *Continental Shelf Research*, *7*, 957–974. https://doi.org/10.1016/0278-4343(87)90008-2

Huthnance, J. M. (1992). Extensive slope currents and the ocean-shelf boundary. *Progress in Oceanography*, *29*(2), 161–196. https://doi.org/10.1016/0079-6611(92)90023-S

Huthnance, J. M. (2004). Ocean-to-shelf signal transmission: A parameter study. *Journal of Geophysical Research*, *109*, C12029. https://doi.org/10.1029/2004JC002358

Isoguchi, O., & Kawamura, H. (2006). Seasonal to interannual variations of the western boundary current of the subarctic North Pacific by a combination of the altimeter and tide gauge sea levels. *Journal of Geophysical Research*, *111*, C04013. https://doi.org/10.1029/2005JC003080

Jan, S., Wang, J., Chern, C.-S., & Chao, S.-Y. (2002). Seasonal variation of the circulation in the Taiwan Strait. *Journal of Marine Systems*, *35*, 249–268. https://doi.org/10.1016/s0924-7963(02)00130-6

Kalnay, E., Kanamitsu, M., Kistler, R., Collins, W., Deaven, D., Gandin, L., et al. (1996). The NCEP/NCAR 40-Year Reanalysis Project. *Bulletin of the American Meteorological Society*, *77*(3), 437–471. https://doi.org/10.1175/1520-0477(1996)077<0437:tnyrp>2.0.co;2

LeBlond, P. H., & Mysak, L. A. (1978). *Waves in the ocean* (p. 602). Elsevier.

Lee, T., Fournier, S., Gordon, A. L., & Sprintall, J. (2019). Maritime Continent water cycle regulates low-latitude chokepoint of global ocean circulation. *Nature Communications*, *10*, 2739. https://doi.org/10.1038/s41467-019-10109-z

Li, P., & Xu, F. (2020). Understanding and reconstructing the coastal sea level variations along the western boundary of the North Pacific. *Geoscience Letters*, *7*, 5. https://doi.org/10.1186/s40562-020-00153-9

Lin, H., Thompson, K. R., Huang, J., & Veronneau, M. (2015). Tilt of mean sea level along the Pacific coasts of North America and Japan. *Journal of Geophysical Research: Oceans*, *120*, 6815–6828. https://doi.org/10.1002/2015JC010920

Lin, W., Lin, H., & Hu, J. (2021). The tilt of mean dynamic topography and its seasonality along the coast of the Chinese mainland. *Journal of Geophysical Research: Oceans*, *126*, e2020JC016778. https://doi.org/10.1029/2020JC016778

Middleton, J. H. (1987). Steady coastal circulation due to oceanic alongshore pressure gradients. *Journal of Physical Oceanography*, *17*(5), 604–612. https://doi.org/10.1175/1520-0485(1987)017<0604:sccdto>2.0.co;2

Minobe, S., Terada, M., Qiu, B., & Schneider, N. (2017). Western boundary sea level: A theory, rule of thumb, and application to climate models. *Journal of Physical Oceanography*, *47*, 957–977. https://doi.org/10.1175/JPO-D-16-0144.1

Monserrat, S., Vilibić, I., & Rabinovich, A. B. (2006). Meteotsunamis: Atmospherically induced destructive ocean waves in the tsunami frequency band. *Natural Hazards and Earth System Sciences*, *6*, 1035–1051. https://doi.org/10.5194/nhess-6-1035-2006

Munk, W. H. (1950). On the wind-driven ocean circulation. *Journal of the Atmospheric Sciences*, *7*(2), 79–93. https://doi.org/10.1175/1520-0469(1950)007<0080:otwdoc>2.0.co;2

Oey, L. Y., Chang, Y. L., Lin, Y. C., Chang, M. C., Varlamov, S., & Miyazawa, Y. (2014). Cross flows in the Taiwan Strait in winter. *Journal of Physical Oceanography*, *44*, 801–817. https://doi.org/10.1175/JPO-D-13-0128.1

Pedlosky, J. (1996). *Ocean circulation theory* (p. 453). Springer.

Piecuch, C. G., Bittermann, K., Kemp, A. C., Ponte, R. M., Little, C. M., Engelhart, S. E., & Lentz, S. J. (2018). River-discharge effects on United States Atlantic and Gulf coast sea-level changes. *Proceedings of the National Academy of Sciences of the United States of America*, *115*(30), 7729–7734. https://doi.org/10.1073/pnas.1805428115

Piecuch, C. G., & Wadehra, R. (2020). Dynamic sea level variability due to seasonal river discharge: A preliminary global ocean model study. *Geophysical Research Letters*, *47*, e2020GL086984. https://doi.org/10.1029/2020GL086984

Qiu, B. (2002). Large-scale variability in the midlatitude subtropical and subpolar North Pacific Ocean: Observations and causes. *Journal of Physical Oceanography*, *32*(1), 353–375. https://doi.org/10.1175/1520-0485(2002)032<0353:lsvitm>2.0.co;2

Qiu, B. (2003). Kuroshio extension variability and forcing of the Pacific Decadal Oscillations: Responses and potential feedback. *Journal of Physical Oceanography*, *33*(12), 2465–2482. https://doi.org/10.1175/2459.1

Saha, S., Moorthi, S., Pan, H., Wu, X., Wang, J., Nadiga, S., et al. (2010). The NCEP Climate Forecast System Reanalysis. *Bulletin of the American Meteorological Society*, *91*(8), 1015–1058. https://doi.org/10.1175/2010BAMS3001.1

Skeel, R. D., & Berzins, M. (1990). A method for the spatial discretization of parabolic equations in one space variable. *SIAM Journal on Scientific and Statistical Computing*, *11*, 1–32. https://doi.org/10.1137/0911001

Stammer, D. (1997). Steric and wind-induced changes in TOPEX/POSEIDON large-scale sea surface topography observations. *Journal of Geophysical Research*, *102*, 20987–21009. https://doi.org/10.1029/97JC01475

Stommel, H. (1948). The westward intensification of wind-driven ocean currents. *Transactions-American Geophysical Union*, *29*, 202–206. https://doi.org/10.1029/TR029i002p00202

Stommel, H., & Leetmaa, A. (1972). Circulation on the continental shelf. *Proceedings of the National Academy of Sciences of the United States of America*, *69*(11), 3380–3384. https://doi.org/10.1073/pnas.69.11.3380

Sverdrup, H. U. (1947). Wind-driven currents in a baroclinic ocean; with application to the equatorial currents of the eastern Pacific. *Proceedings of the National Academy of Sciences of the United States of America*, *33*(11), 318–326. https://doi.org/10.1073/pnas.33.11.318

Vivier, F., Kelly, K. A., & Thompson, L. (1999). Contributions of wind forcing, waves, and surface heating to sea surface height observations in the Pacific Ocean. *Journal of Geophysical Research*, *104*, 20767–20788. https://doi.org/10.1029/1999JC900096

Wang, O., Lee, T., Piecuch, C. G., Fukumori, I., Fenty, I., Frederikse, T., et al. (2022). Local and remote forcing of interannual sea-level variability at Nantucket Island. *Journal of Geophysical Research: Oceans*, *127*, e2021JC018275. https://doi.org/10.1029/2021JC018275

Wise, A., Hughes, C., & Polton, J. (2018). Bathymetric influence on the coastal sea level response to ocean gyres at Western boundaries. *Journal of Physical Oceanography*, *48*, 2949–2964. https://doi.org/10.1175/JPO-D-18-0007.1

Wise, A., Hughes, C. W., Polton, J. A., & Huthnance, J. M. (2020). Leaky slope waves and sea level: Unusual consequences of the beta effect along western boundaries with bottom topography and dissipation. *Journal of Physical Oceanography*, *50*(1), 217–237. https://doi.org/10.1175/JPO-D-19-0084.1

Woodworth, P. L., Melet, A., Marcos, M., Ray, R., Wöppelmann, G., Sasaki, Y. N., et al. (2019). Forcing factors affecting sea level changes at the coast. *Surveys in Geophysics*, *40*, 1351–1397. https://doi.org/10.1007/s10712-019-09531-1

Wright, D. G. (1986). On quasi-steady shelf circulation driven by along-shelf wind stress and open-ocean pressure gradients. *Journal of Physical Oceanography*, *16*, 1712–1714. https://doi.org/10.1175/1520-0485(1986)016<1712:oqsscd>2.0.co;2

Wu, H. (2021). Beta-plane arrested topographic wave as a linkage of open ocean forcing and mean shelf circulation. *Journal of Physical Oceanography*, *51*(3), 879–893. https://doi.org/10.1175/JPO-D-20-0195.1

Wunsch, C., & Stammer, D. (1997). Atmospheric loading and the oceanic "inverted barometer" effect. *Reviews of Geophysics*, *35*, 79–107. https://doi.org/10.1029/96RG03037

Yang, J. Y., & Chen, K. (2021). The role of wind stress in driving the along-shelf flow in the northwest Atlantic Ocean. *Journal of Geophysical Research: Oceans*, *126*, e2020JC016757. https://doi.org/10.1029/2020JC016757

Zhai, X. M., Johnson, H. L., & Marshall, D. P. (2010). Significant sink of ocean-eddy energy near western boundaries. *Nature Geoscience*, *3*, 609–612. https://doi.org/10.1038/ngeo943